

Mechanical and Tribological Properties of HVOF-Sprayed ($\text{Cr}_3\text{C}_2\text{-NiCr+Ni}$) Composite Coating on Ductile Cast Iron

Marzanna Ksiazek, Lukasz Boron, Marta Radecka, Maria Richert, and Adam Tchorz

(Submitted November 5, 2015; in revised form June 29, 2016; published online July 14, 2016)

The aim of the investigations was to compare the microstructure, mechanical, and wear properties of $\text{Cr}_3\text{C}_2\text{-NiCr+Ni}$ and $\text{Cr}_3\text{C}_2\text{-NiCr}$ coatings deposited by HVOF technique (the high-velocity oxygen fuel spray process) on ductile cast iron. The effect of nickel particles added to the chromium carbide coating on mechanical and wear behavior in the system of $\text{Cr}_3\text{C}_2\text{-NiCr+Ni/ductile cast iron}$ was analyzed in order to improve the lifetime of coated materials. The structure with particular emphasis of characteristic of the interface in the system of *composite coating ($\text{Cr}_3\text{C}_2\text{-NiCr+Ni}$)/ductile cast iron* was studied using the optical, scanning, and transmission electron microscopes, as well as the analysis of chemical and phase composition in microareas. Experimental results show that HVOF-sprayed $\text{Cr}_3\text{C}_2\text{-NiCr+Ni}$ composite coating exhibits low porosity, high hardness, dense structure with large, partially molten Ni particles and very fine Cr_3C_2 and Cr_7C_3 particles embedded in NiCr alloy matrix, coming to the size of nanocrystalline. The results were discussed in reference to examination of bending strength considering cracking and delamination in the system of *composite coating ($\text{Cr}_3\text{C}_2\text{-NiCr+Ni}$)/ductile cast iron* as well as hardness and wear resistance of the coating. The composite structure of the coating provides the relatively good plasticity of the coating, which in turn has a positive effect on the adhesion of coating to the substrate and cohesion of the composite coating ($\text{Cr}_3\text{C}_2\text{-NiCr+Ni}$) in wear conditions.

Keywords $\text{Cr}_3\text{C}_2\text{-NiCr}$ coating, HVOF, thermal spraying, wear resistant

1. Introduction

High-velocity oxy-fuel (HVOF) is one of the technologies, which formed coating such as $\text{Cr}_3\text{C}_2\text{-NiCr}$ and WC-Co with very small porosity (a few %), high adhesion strength (above 80 MPa), high hardness, wear resistance, thermal stability, and corrosion resistance, and many more carbide particles remain in matrix compared with the plasma spraying process (Ref 1-3). High wear resistance, hardness, thermal conductivity, and excellent wettability of chromium carbide by NiCr alloy and strong adhesion between phases has caused the $\text{Cr}_3\text{C}_2\text{-NiCr}$ coatings to become one of the promising materials for use on highly loaded components made of ductile cast iron in the automotive and aerospace industries. In particular, chromium carbide-based materials are frequently used for many of the applications in gas turbine, steam turbine, and aeroengine to improve the resistance to sliding, abrasive, and erosive wear (Ref 4, 5). $\text{Cr}_3\text{C}_2\text{-NiCr}$ coatings offer greater corrosion and

oxidation resistance, also having a high melting point and maintaining high hardness, strength, and wear resistance up to a maximum operating temperature of 900 °C. In addition to these features, the coefficient of thermal expansion of Cr_3C_2 ($10.3 \times 10^{-6}/^\circ\text{C}$) is nearly similar to that of iron ($11.4 \times 10^{-6}/^\circ\text{C}$) and nickel ($12.8 \times 10^{-6}/^\circ\text{C}$) that constitute the base of most high temperature alloys. This minimizes stress generation through thermal expansion mismatch during thermal cycles (Ref 6, 7). However, their abrasive and erosive wear resistance at room temperature is lower than that of WC-based coating. Therefore, research is still in progress to improve the performance of coatings, in particular, the resistance to wear and high temperature corrosion.

They can be increased by modification of the chemical composition of the ceramic powders, by admixture of metal particles or through additional process steps after spraying. There are only few studies dealing with coating composition of the HVOF-sprayed $\text{Cr}_3\text{C}_2\text{-based}$ coating, that are focused on optimizing the content of chromium carbide in the presprayed coatings. It has been found that the addition of Cr, Co, B, and Ni to $\text{Cr}_3\text{C}_2\text{-NiCr}$ coating inhibits to a large extent the decomposition of Cr_3C_2 as well as having a beneficial effect on the wear resistance and fracture toughness (Ref 8, 9). Moreover, the studies have shown that an increase in decarburization of $\text{Cr}_3\text{C}_2\text{-NiCr}$ coating will decrease the abrasion resistance and increases the hardness of the coating because it introduces undesirable brittle phases (Ref 10), which leads to decreases its durability.

The objective of the work was to determine the effect of Ni particles added to the HVOF-sprayed $\text{Cr}_3\text{C}_2\text{-NiCr}$ coating on mechanical and wear properties, in order to improve the lifetime of coated material—ductile cast iron, and characterize microstructural changes by both scanning and transmission microscopy.

This article is an invited submission to JMEP selected from presentations at the Symposium “Metal-Matrix Composites,” belonging to the topic “Composite and Hybrid Materials” at the European Congress and Exhibition on Advanced Materials and Processes (EUROMAT 2015), held September 20-24, 2015, in Warsaw, Poland, and has been expanded from the original presentation.

Marzanna Ksiazek, Lukasz Boron, and Adam Tchorz, Foundry Research Institute, 73 Zakopianska St., 30-418 Kraków, Poland; and Marta Radecka and Maria Richert, AGH University of Science and Technology, 30 Mickiewicza Ave., 30-059 Kraków, Poland. Contact e-mail: marzanna.ksiazek@iod.krakow.pl.

2. Experimental Procedure

2.1 Materials

In this study, ductile cast iron EN-GJS-500-7 (3.61% C, 2.29% Si, 0.45% Mn, 0.045% P, 0.009% S, 0.03% Cr, 0.01% Ni, 0.057% Mg, 0.75% Cu rest of Fe) was used as a substrate. The ductile iron specimens of $100 \times 15 \times 5$ mm were sand-blasted using 20 mesh alumina grits to a surface roughness of about R_a 5.8 μm prior to deposition. The ductile cast iron substrate had the following mechanical properties: $R_m = 500$ MPa, $R_{p0.2} = 340$ MPa, $A_5 = 7\%$, 220 HB. Then the composite ceramic powder (Cr_3C_2 -75 wt.% NiCr +10 wt.% Ni) was deposited by a commercial HVOF spraying equipment (HV-50 HVOF System in Plasma System S.A.), using kerosene and oxygen as fuel. The particle size of the powder Cr_3C_2 -75 wt.% NiCr was 45–60 μm , the size of Ni particles introduced to the powder was 20 μm and the average thickness of the coating was about 200 μm . The spraying parameters for HVOF spraying are shown in Table 1.

2.2 Test Procedures

The morphological and microstructural examinations of the system-type *coating/substrate* were carried out in light microscopy (LM), scanning electron microscopy (SEM), and transmission electron microscopy (TEM). The measurements of the chemical composition in the coating/substrate zone were carried out using a Link ISIS 300 Energy Dispersive X-ray Spectrometer (EDS) attached to a STEREOSCAN scanning electron microscopy operating at 20 kV voltage. The TEM examinations (JOEL 2010 ARP transmission electron microscope equipped with Energy Dispersive X-ray Spectrometer) of the structure of the coating/substrate specimens were made on thin foils in a Gatan PIPS691V3.1 ion thinner by standard methods, i.e., by cutting out 3-mm-diameter disk thinning by dimpler, and ion polishing (Ref 11). Structural analysis was performed by means of XRD within the angular range of 20–90° degree on a X'Pert Pro Panalytical diffractometer with CuK radiation. Phase identification was carried out with the help of ICDD database. Based on Rietveld analysis of XRD data with the use of GSAS/EXPGUI set of software, phase composition was derived. The average crystallite size was calculated from the Scherrer formula upon taking into account the instrumental broadening.

Porosity of the composite coating was measured on microscopic images (LM) with the Aphelion 3.0 software for analyzing stereological parameters of the microstructure.

Coating microhardness was measured using Vickers method, by means of Hanemann microhardness meter installed on Neophot 2 microscope under a 1N load on the cross sections of normal samples relative to their surfaces. The roughness of the coated sample was measured by the contact method on Hammel Tester T500 of Hommelwerker Company GmbH.

Bond strength of the system *Cr₃C₂-NiCr+Ni/ductile iron* was measured using a 3-point bend test on INSTRON 8800M machine with especially device designed to perform detailed

studies of the fracture properties. Test specimens were prepared as beams, $100 \times 15 \times 5$ mm with the top surface coated and the other sides polished. Specimens were tested using three-point bending with a spacing supports of 70 mm with automatic recording of applied load versus the corresponding displacement up to failure under a constant load displacement rate of 1 mm/min. All bend test results represent the average of at least three measurements. The cracks resulting from the bend tests were studied with SEM.

Tribological testing was performed using a scratch tester with Rockwell C diamond indenter with a radius 50 μm . The test was performed using Micro-Combi-Tester device made by Swiss company CMS. The length of the scratch was 5 mm. The changes of loading for the coatings were linear, and the range over the entire scratch length was 0.9 to 45 N. The indenter was moved at a speed 5 mm/min. The parameters measured during the test were the indenter penetration depth, force applied to it, the tangential force, and acoustic emission. Previous studies have shown that the adhesion of a coating to the substrate can be determined by scratch testing using progressive loading (Ref 12, 13). The technique involves generating a controlled scratch with a tip on the sample. The tip, made of diamond is drawn across the surface under progressive load. At a certain load, the material will start to fall. The critical loads are determined by means of investigation of optical observation, the coefficient of friction as the ratio of frictional force to the applied force (F_t/F_n), penetration depth (P_d), and acoustic emission (A_e).

3. Results and Discussion

3.1 Structural Characterisation of the *Cr₃C₂-NiCr+Ni/Ductile Cast Iron System*

The typical microstructures of the HVOF-sprayed chromium carbide coating with Ni particles on a ductile cast iron are shown in Fig. 1. The coatings consisted of lamellae elongated in the direction parallel to coating surface. The structure of the Cr_3C_2 -NiCr+Ni coating consists of fine undeformed grains of chromium carbide, which are embedded in NiCr alloy matrix, and large, partially molten Ni particles (not fully molten) which—while hitting the substrate—change their shape from spherical to elongated, change their height, and elongate in parallel to the coating surface. The cross section and top surface of the both coatings exhibited dense microstructure with high cohesion, without cracks, due to the high impact velocity of the coating particles. However, a few pores appears with black color in the micrographs. Porosity of the composite coating is $4.2 \pm 0.2\%$ and for coating produced with conventional powder is 6% (resulting from higher porosity of the grains). Addition of Ni tended to reduce porosity (in particular as regards the number and size of pores) of the coating because compared Cr_3C_2 , Ni has lower melting point and easier to be melted, which can fill the pores in the coating. As confirmed by previous research findings, the porosity resulting from incomplete melting during deposition reduces the strength of the

Table 1 HVOF spraying conditions

Feed rate, mm/s	Oxygen, L/min	Kerosene, L/h	Powder feed rate, g/min	Powder feed gas, L/min	Spraying distance, mm
583	944	25.5	92	Nitrogen, 9.5	370

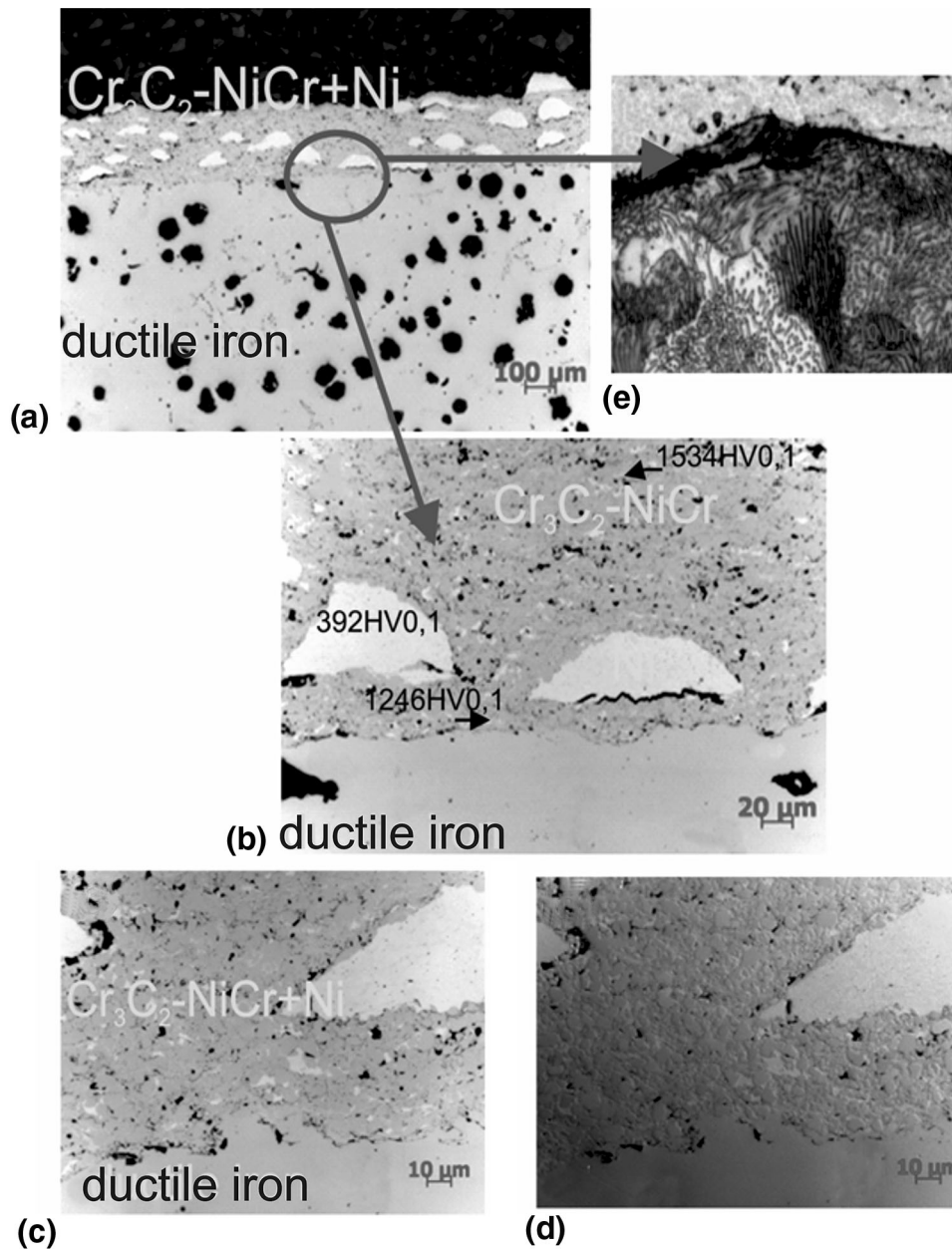


Fig. 1 (a) Microstructure of the $\text{Cr}_3\text{C}_2\text{-NiCr+Ni}$ /ductile cast iron interface, (b) magnified area selected in (a), (c, d) details of the coating structure in differential interference contrast (DIC), and (e) cast iron structure composed of ferrite and pearlite

individual lamellae (Ref 5, 10). Moreover, in the cast iron structure, in particular at the *coating-substrate* interface, no changes after spraying process were observed (initial and postspraying matrix of the cast iron is composed of ferrite and pearlite, Fig. 1e). No diffusion of elements from the substrate material to the coating and opposite was found, which indicates the adhesive mechanism of the bonding between the coating material and substrate.

The microhardness of the composite coating $\text{Cr}_3\text{C}_2\text{-NiCr+Ni}$ on ductile cast iron is varied and, for a measuring point located at the depth 30 μm from the coating surface, it is 1534HV0,1, for the point located at the coating-substrate interface, it is 1246HV0,1, and then decreases to the value of 230HV0,1 for the substrate. Note that there is a great difference between the hardness of the Ni particle (392HV0,1) and carbide particles

(1200-1500HV0,1). Additive of metallic particles locally reduced of the coating hardness which, in turn leads to reduced brittleness. Additionally, the reduction of microhardness is usually associated with high modulus of elasticity, causes the coating becomes more plastically (Ref 14). It is worth noting at this point that, after thermal spraying of composite coating on ductile cast iron, 6-fold increase in hardness of the cast iron is observed, compared to the initial state, i.e., without the coating.

Figure 2 presents a SEM micrograph of a representative region of the $\text{Cr}_3\text{C}_2\text{-NiCr+Ni}$ coating cross section showing the typical microstructure, which consists of fine (from micrometric to submicrometric) Cr_3C_2 grains are surrounded by a matrix (NiCr). A large part of fine grains in the coating material indicates an increase of plasticity of the coating owing to slipping the grain boundaries. SEM images are shown the

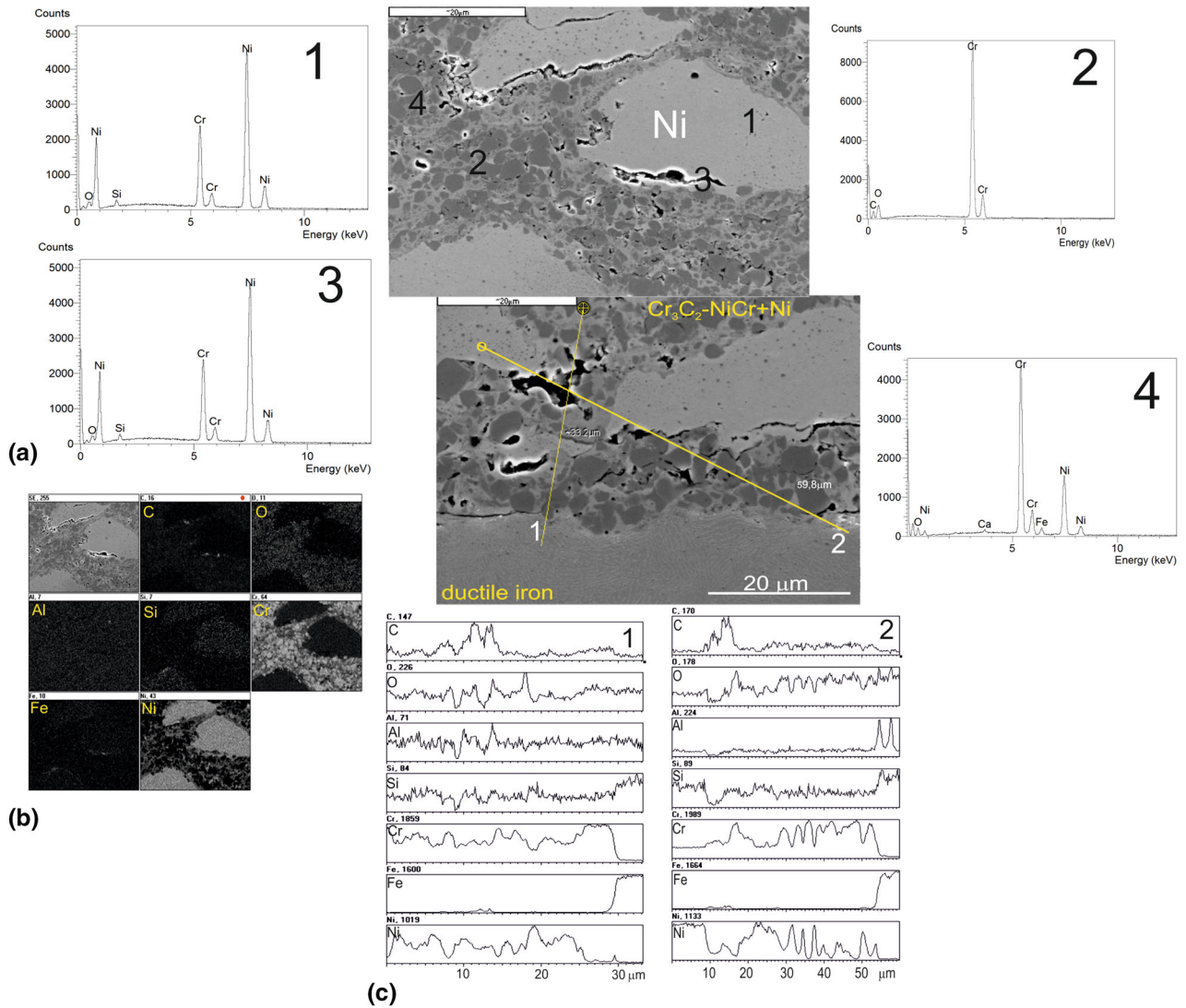


Fig. 2 (a) Scanning micrographs of the Cr_3C_2 -NiCr+Ni/ductile cast iron interface with EDS spectra taken from the marked points: 1, 2, 3, and 4, (b) map of distribution of concentrations of C, O, Al, Si, Cr, Fe, Ni taken from the region of interface (c) linear distribution of C, O, Al, Si, Cr, Fe, and Ni

mapping of elements revealed the presence of elements in the coating (Fig. 2b), linear changes of composition (Fig. 2c), and the point analysis of composition in individual phases of Cr_3C_2 , NiCr and Ni. Darker regions are identifiable, consisting of micrometric Cr_3C_2 grains (Fig. 2a, label 2). On the other hand, brighter Ni and NiCr containing regions exist, respectively (Fig. 2a, label 1, 4).

Detailed microstructural tests of the coating on thin film of cross-sectional TEM sample proved nanocrystalline structure with striped character. In the coating microstructure, elongated 20-50-nm-thick bands of Cr_3C_2 particles arranged in parallel are found (Fig. 3). Electron diffraction ring patterns proved the nanocrystalline nature of the coating structure. Point analysis of the chemical composition was obtained with the energy dispersive X-ray spectroscopy (EDS) technique, and identified elements contained in the coating: Cr, C, and Ni.

X-ray diffraction patterns for Cr_3C_2 -NiCr+Ni coated sample is shown in Fig. 4. As it can be observed, the main phases present in the sprayed coating were Cr_3C_2 , and NiCr phases. Apart from Cr_3C_2 carbides particles, the carbide Cr_7C_3 was also present in the X-ray diffraction analyses. Evidently, the

decarburation (partial decomposition) Cr_3C_2 results in formation of Cr_7C_3 , owing overheating of the particles during the spraying process. The matrix consists of a NiCr and small amount of Ni-rich phase (Ni_3Cr) as a result of supersaturation. Accordingly, in the XRD pattern of this coating peak of Ni_3Cr is hardly recognizable, while those of NiCr are more intense. Additionally, volume fractions of individual phases in the coating examined were determined (Table 2). X-ray diffraction analysis confirmed the presence of a larger percentage of Cr_3C_2 (a highest peak shows presence of pure chromium carbide). This result show that due to the higher flame velocity and lower flame temperature of the HVOF process, the decomposition process is limited. The contents of each phase are presented in Figure: the Cr_3C_2 content was 59.4 wt.%, the fractions of Cr_7C_3 was 8.1 wt.%, and Ni_3Cr phase was 3.3 wt.%, while the NiCr value amounted to 29.2 wt.%. It is worth to emphasize that the precipitation of Cr_7C_3 in the NiCr matrix resulting from Cr_3C_2 decarburation can modify the microstructure of the coating and consequently improves the wear resistance. The level of decarburation of Cr_3C_2 has also been found to play an important role in relation to both hardness and wear properties

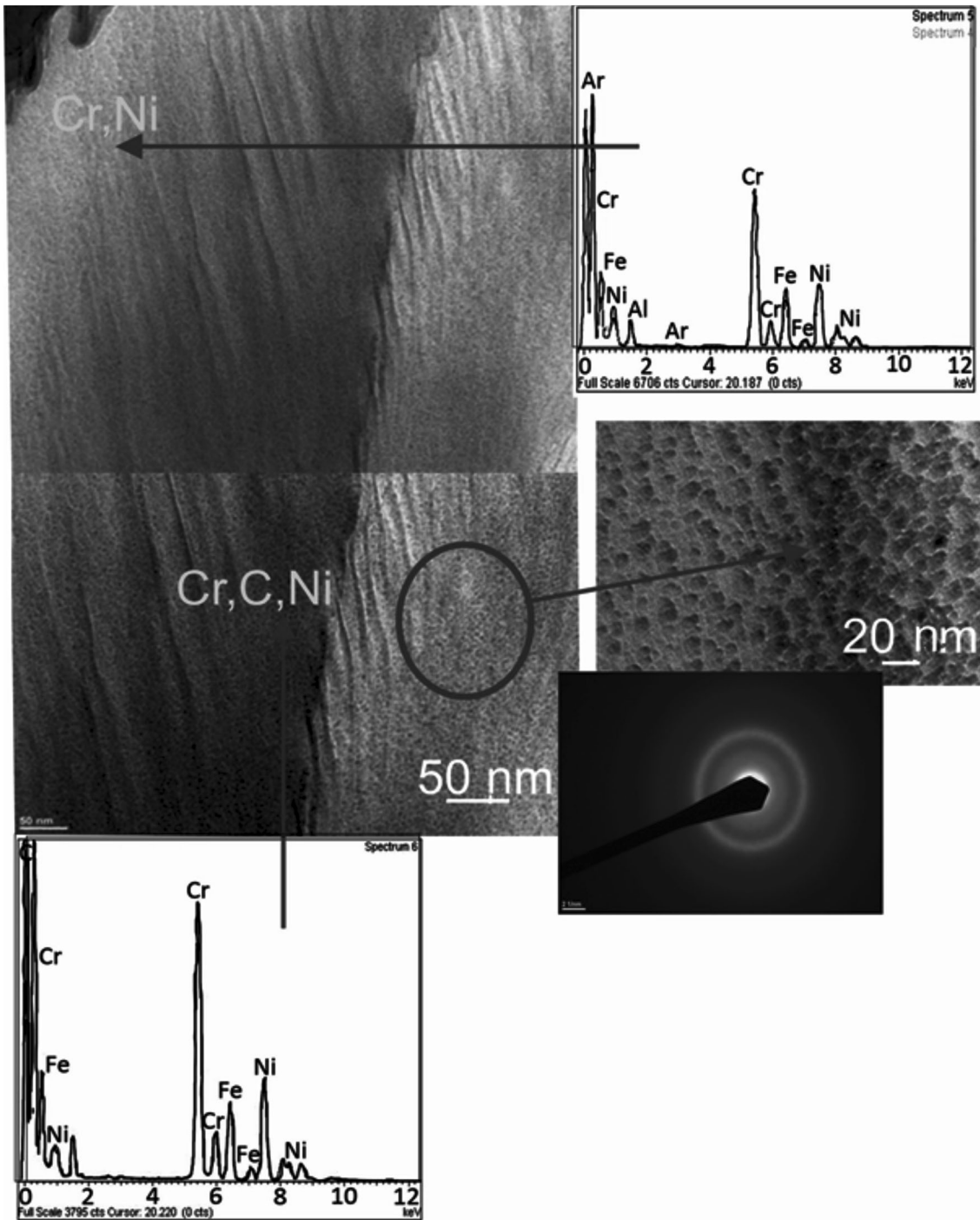


Fig. 3 TEM analysis of the composite coating ($Cr_3C_2-NiCr+Ni$) with corresponding EDS spectra and representative area diffraction pattern indicates the formation of nanocrystalline structure

of coatings, since a high hardness is required in order to improve the coating wear performance. In addition, nanostructured carbide phases can be improved fracture toughness of the coating (by enhancing crack propagation resistance).

3.2 Mechanical Characterisation of the $Cr_3C_2-NiCr+Ni$ /Ductile Cast Iron System

Figure 5 compares the results of a bending test for Cr_3C_2-NiCr /ductile cast iron, $Cr_3C_2-NiCr+Ni$ /ductile cast iron sys-

tems, and ductile cast iron. In the systems studied, bending curves are parabolic. For the $Cr_3C_2-NiCr+Ni$ /ductile cast iron system, a longer deflection path occurs, during which the stress increases gently and then it decreases. The deflection value at which the stress reduction causing sample damage occurs is approximately 3.9 mm. However, for the Cr_3C_2-NiCr /ductile cast iron system, there is no such a long range of the deflection path. Comparing the curves obtained, it can be concluded that for the Cr_3C_2-NiCr /ductile cast iron system, a slight reduction of force parameters of the bending process

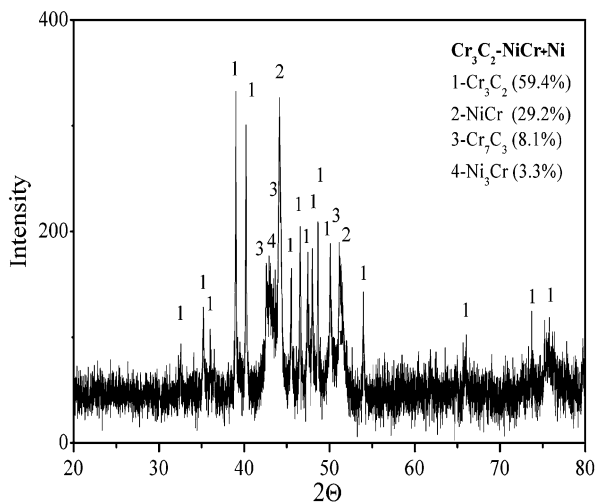


Fig. 4 X-ray diffraction pattern of the composite carbide coating ($\text{Cr}_3\text{C}_2\text{-NiCr+Ni}$) deposited by on ductile cast iron by HVOF

Table 2 Detailed results of XRD

Composition	Weight percentage of phase composition, %	Crystal size from XRD D_{XRD} , nm
Cr_3C_2	59.4	50
Cr_7C_3	8.1	24
NiCr	29.2	32
Ni_3Cr	3.3	12

occurs, and the deflection is reduced to the value 2.5 mm. For comparison, the deflection value at which the stress reduction causing sample of substrate damage occurs is approximately 6.0 mm. The bending strength of $\text{Cr}_3\text{C}_2\text{-NiCr+Ni/ductile cast iron}$ system was formed to increase by 20 MPa as compared to that of $\text{Cr}_3\text{C}_2\text{-NiCr/ductile cast iron}$ system. The values of maximum bending stress for $\text{Cr}_3\text{C}_2\text{-NiCr/ductile cast iron}$ and $\text{Cr}_3\text{C}_2\text{-NiCr+Ni/ductile cast iron}$ systems are, respectively, 553 MPa \pm 10 and 573 MPa \pm 12. It can be observed that *coating/substrate* systems are characterized by relatively high strength properties but with decreased plasticity, in particular, for a system with coating free of metallic particles. Moreover, there are changes in size of the individual stages of bending curves, in particular of the linear strengthening and plastic flow, which is reduced for the $\text{Cr}_3\text{C}_2\text{-NiCr/ductile cast iron}$ system. The chromium carbide coating without Ni particles is harder and more brittle, which in turn reduces the dissipation of plastic deformation energy, and the intensely growing load causes crack propagation and reduced deflection range. Also, the rapid solidification during deposition process and the various defects (pores, voids, and microcracks) produce stresses in the coating, which may lead to interlamellae debonding and a weakening of the bond strength between coating and substrate (Ref 2, 6).

Observations of sample fractures after the bending test, performed with a scanning microscope (Fig. 6) show a different damage mechanism, depending on the structure and phase composition of a coating. For the $\text{Cr}_3\text{C}_2\text{-NiCr/ductile cast iron}$ system, the damage occurs along the coating-substrate interface, with affecting it. However, for the $\text{Cr}_3\text{C}_2\text{-NiCr+Ni/ductile cast iron}$ system, the damage occurs both in the coating near the

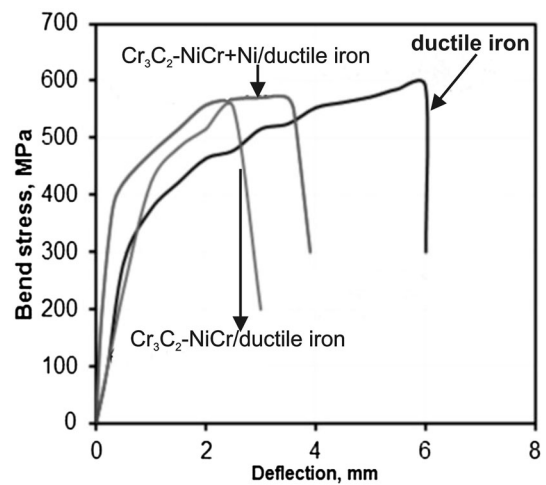


Fig. 5 Bend test curves recorded for the systems type: $\text{Cr}_3\text{C}_2\text{-NiCr/ductile cast iron}$, $\text{Cr}_3\text{C}_2\text{-NiCr+Ni/ductile cast iron}$, and ductile cast iron

coating-substrate interface and along the interface, without affecting it. The fractured surfaces from the bend test were very rough with protruding splats. It was observed that the $\text{Cr}_3\text{C}_2\text{-NiCr+Ni/ductile cast iron}$ system had a rougher fracture surface than the $\text{Cr}_3\text{C}_2\text{-NiCr/ductile cast iron}$ system. This may be due to the fact that the coating material with Ni particles added is more plastic and its resistance to cracking is higher which, in turn causes such material to deform plastically in the crack front, absorb the energy and stop the cracking. It means, that the addition of soft, metallic particles to the coating minimized the damage to the surface of the coating. Moreover, fine structure and developed surface of the coating fracture indicate its good resistance to cracking.

Generally, during the scratch test, no large cracks were observed in the both coatings. The resistance to wear of all tested coatings is approximately the same. However, the scratch trace in case of the composite coating shows microgrooves and plastic deformation (Fig. 7). In Fig. 7, it can be seen that the failure is quantified by a sudden drop in the depth signal (P_d) and by an emission acoustic (A_e); the two datasets being indicators of failure can then be correlated to actual damage seen via optical microscopy. Table 3 presents the values of critical load which corresponds to the appearance of first slight cracks in the coatings examined and adhesion cracks, as well as the maximum indenter penetration depths. For the composite $\text{Cr}_3\text{C}_2\text{-NiCr+Ni}$ coating, initially slight cohesive cracks were observed at the loading of 13.5 N, for $\text{Cr}_3\text{C}_2\text{-NiCr}$ coating at the loading of 10 N. The values of the loading were considered as the L_{c1} . For the composite $\text{Cr}_3\text{C}_2\text{-NiCr+Ni}$ coating, complete layer damage was observed at the loading 25 N, for Cr_3C_2 coating at the loading 23 N (adhesive cracking). It should be pointed out, that the critical load usually increase with substrate hardness and decreases with increasing surface roughness (Ref 15). Lower value of the critical damage for the carbide chromium coating relative to the coating with Ni indicates its greater brittleness. Furthermore, the indenter penetration depth was lower for the $\text{Cr}_3\text{C}_2\text{-NiCr}$ coating, which is due to a higher microhardness of this layer over its cross section. Moreover, increasing plasticity of the $\text{Cr}_3\text{C}_2\text{-NiCr}$ coating by addition of 10% Ni particles to the coating material contributes to reduced wear.

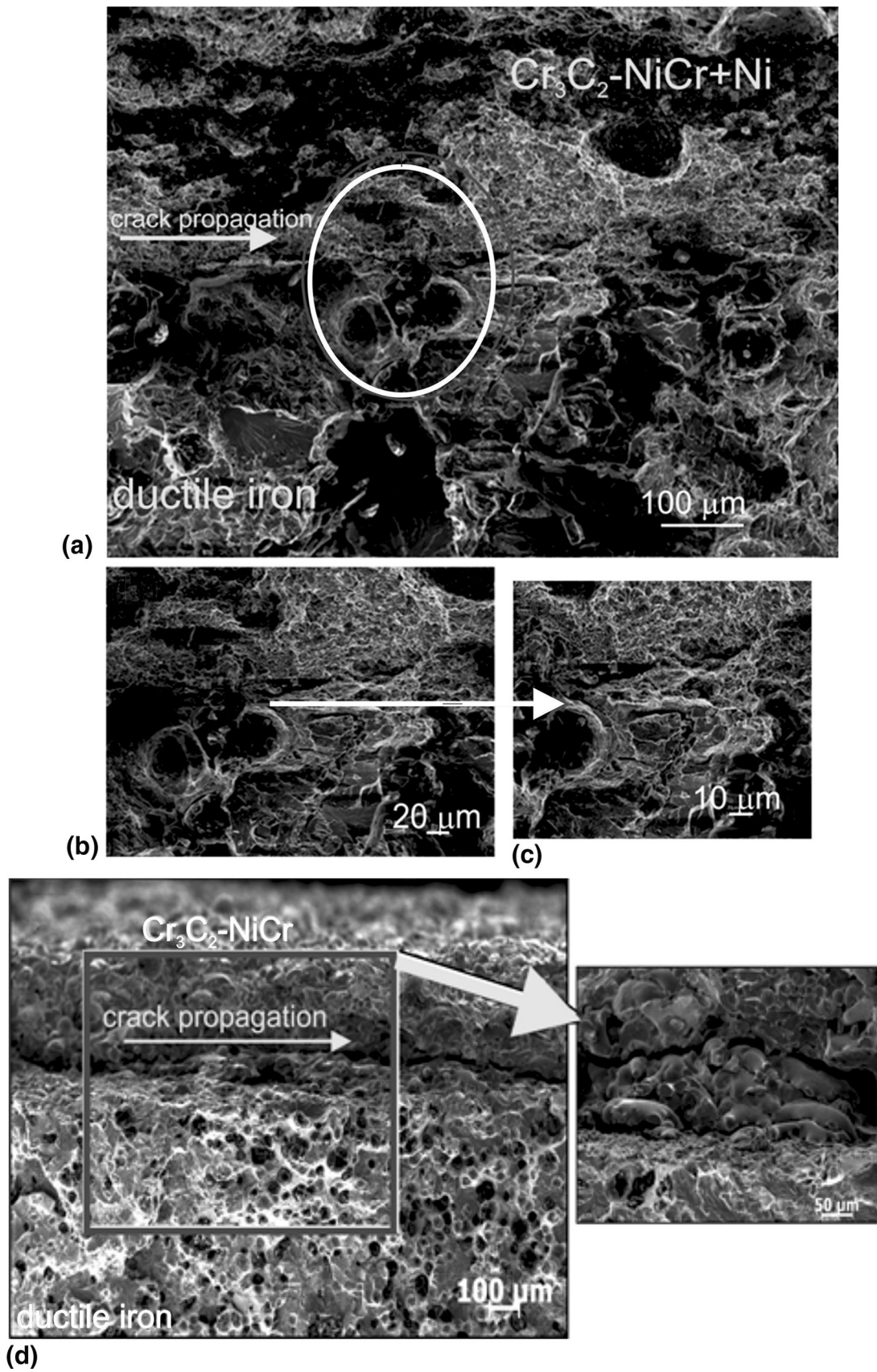


Fig. 6 Scanning micrographs of the fracture surface after bend test for the systems type: (a) $\text{Cr}_3\text{C}_2\text{-NiCr+Ni}$ /ductile cast iron, (b, c) magnified area selected in (a) and (d) $\text{Cr}_3\text{C}_2\text{-NiCr}$ /ductile cast iron with magnified area selected in (d)

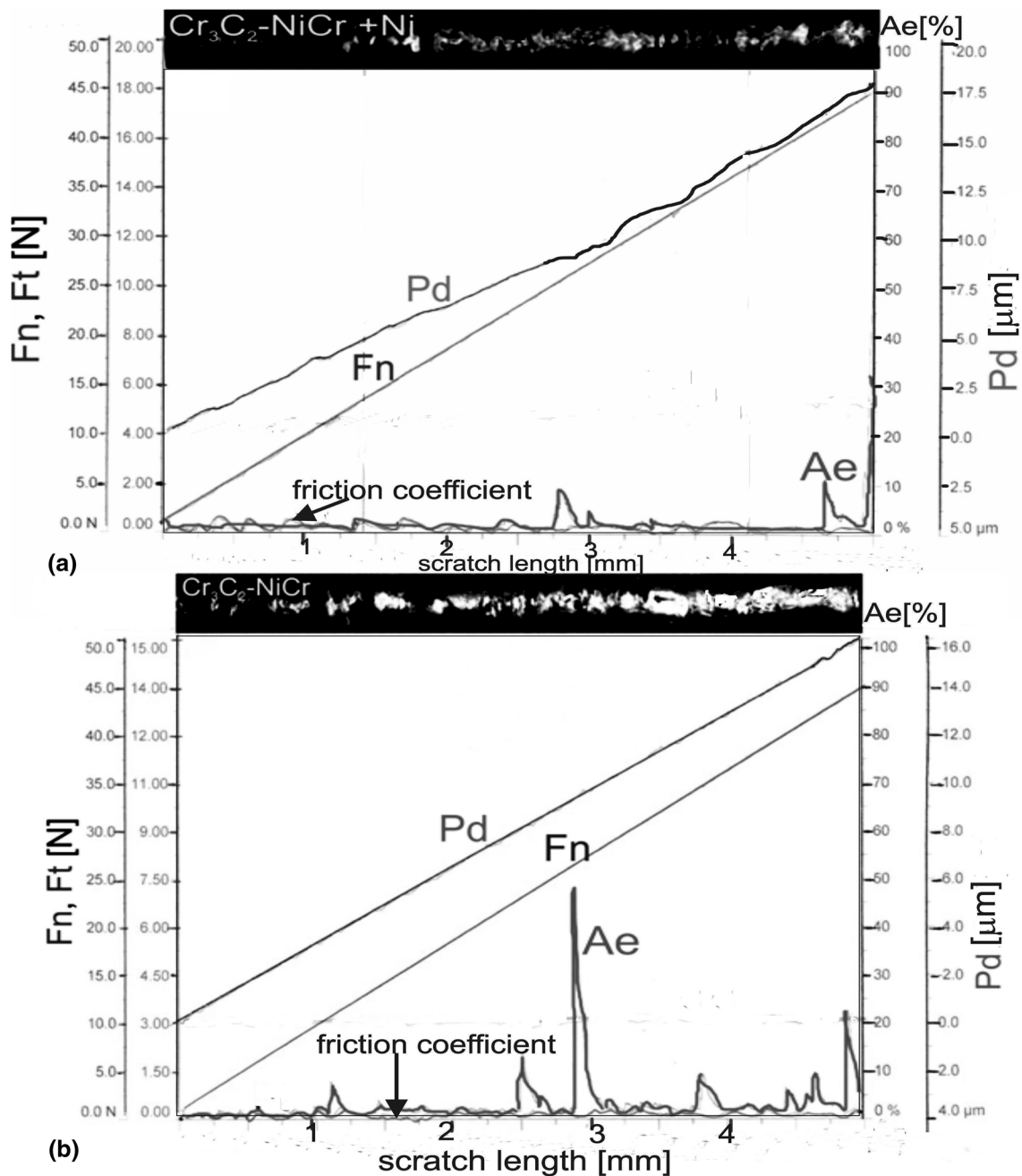


Fig. 7 Results: F_n -Normal force, Friction coefficient—as characteristic of a friction force F_t , P_d -Penetration depth, and A_e -Acoustic emission obtained from the scratch test for a present force of 1- 45 N with the line of surface scratching for the systems type: (a) Cr_3C_2 -NiCr+Ni/ductile cast iron and (b) Cr_3C_2 -NiCr/ductile cast iron

Table 3 Scratch test results for layered systems

Coatings	Observed wear			
	Layer cracks with large delamination areas			
	L_{C1} , N	h_{C1} , μm	L_{C2} , N	h_{max} , μm
Cr_3C_2 -NiCr	10.0 ± 0.6	4.0 ± 0.2	23.0 ± 0.8	16.3 ± 0.6
Cr_3C_2 -NiCr+Ni	13.5 ± 0.8	5.0 ± 0.2	25.5 ± 1.5	17.7 ± 0.9

L_{C1} cohesive crack of the coating, L_{C2} adhesion crack in the scratch track, h_{C1} indenter penetration depth at L_{C1} , h_{C2} indenter penetration depth at max. loading 45 N

The significant influence on the wear of the coating has its roughness, porosity, and the phase composition of coating. It is worth mentioning that coating with Ni particles on ductile cast iron is characterized by relatively high surface roughness, the roughness value R_a (center line average height) is 10.0 μm and relatively low porosity. For the coating without Ni particles, the roughness value R_a is 6.6 μm (Cr_3C_2 -NiCr coatings show a smooth surface without microparticles in the form of droplets). The splat densification level and the corresponding roughness of the composite coatings are mainly affected by the particle velocity and the molten state of the sprayed particles. The difference in size of powder metal and ceramic as well as differences in the flow of the molten material after impact the powder particles to the substrate also affect the surface roughness. In addition to the microstructural features of the studied coatings, the size and shape of Ni particles in the carbide coating causes plasticity of coating and which in turn provides less damage of the surface. As confirmed by previous research findings, the wear resistance of a coated material with smooth surface is expected to decrease (Ref 16). Moreover, soft particles of Ni compared with the hardness of the carbide phase and weakly associated with it, may cause the lubricating effect by grinding on the surface of the machined material. A significant impact on the process of wear of composite coatings has both the size and distribution of the carbide particles and Ni particles as well as the hardness of these phases.

4. Conclusion

From the experimental results, the following conclusions can be drawn:

1. The composite carbide coating Cr_3C_2 -NiCr+Ni deposited on ductile iron by HVOF technique is characterized by low porosity, dense structure, good adhesion, and high hardness:
 - in the structure of the coating there are large, partially molten Ni particles and fine Cr_3C_2 particles embedded in NiCr alloy matrix, coming to the size of nanocrystalline,
 - within the coating Cr_3C_2 and Cr_7C_3 were present with different morphologies. The precipitation of Cr_7C_3 in the NiCr matrix resulting from Cr_3C_2 decarburization can modify the microstructure of the coating and consequently will strengthen NiCr matrix phase,
 - there was no visible changes in the structure of the substrate which accurately predicts in reference to the applications of produced coatings.
2. The composite structure of the Cr_3C_2 -NiCr+Ni coating provides good resistance to cracking. The failure occurs partly along the *coating-substrate* interface as well as in the coating—do not propagate to the substrate material.
3. The composite carbide coating Cr_3C_2 -NiCr+Ni on ductile iron has good wear resistance associated with the effect of plasticity of the coating by addition of soft, metallic particles to the base ceramic powder. In addition, better wear properties are obtained as the decarburisation degree decreases.

Acknowledgment

The present project was financially supported by the National Science Centre of Poland (Contract No. 2012/07/B/ST8/03778).

Open Access

This article is distributed under the terms of the Creative Commons Attribution 4.0 International License (<http://creativecommons.org/licenses/by/4.0/>), which permits unrestricted use, distribution, and reproduction in any medium, provided you give appropriate credit to the original author(s) and the source, provide a link to the Creative Commons license, and indicate if changes were made.

References

1. P. Sahoo and R. Raghuraman, *Thermal Spray Coatings: Research, Design and Application*, C.C. Berndt and T.F. Bernecki, Ed., ASM International, Materials Park, Ohio, 1993,
2. S. Koruda, T. Dendo, and S. Kitahara, Quenching Stress in Plasma Sprayed Coating and Its Correlation with the Deposit Microstructure, *J. Therm. Spray Technol.*, 1995, **4**, p 75–84
3. W. Fang et al., Processing Optimization, Surface Properties and Wear Behaviour of HVOF Spraying WC-Cr-Cr-Ni Coating, *J. Mater. Process. Technol.*, 2009, **209**, p 561–567
4. B. Yin, G. Lin, H. Zhou, J. Chen, and F. Yan, Sliding Wear Behaviour of HVOF-Sprayed Cr_3C_2 -NiCr/CeO₂ Composite Coatings at Elevated Temperature up to 800 °C, *Tribol. Lett.*, 2010, **37**, p 584–591
5. W. Tillmann, E. Vogli, I. Baumann, G. Kopp, and C. Weihs, Desirability-Based Multi-Criteria Optimization of HVOF Spray Experiments to Manufacture Fine Structured Wear-Resistant $75\text{Cr}_3\text{C}_2$ -25(NiCr₂O) Coatings, *J. Therm. Spray Technol.*, 2010, **19**(1-2), p 392–408
6. S. Kamal, R. Jayaganthan, S. Prakash, and S. Kumar, Hot Corrosion Behaviour of Detonation Gun Sprayed Cr_3C_2 -NiCr Coatings on Ni and Fe-Based Superalloys in Na₂SO₄-60% V₂O₅ Environment at 900 °C, *J. Alloys Compd.*, 2008, **463**, p 358–372
7. M. Roy, A. Pauschitz, R. Polak, and F. Franek, Comparative Evaluation of Ambient Temperature Friction Behaviour of Thermal Sprayed Cr_3C_2 -25(Ni₂₀Cr) Coatings with Conventional and Nano-Crystalline Grains, *Tribol. Int.*, 2006, **39**, p 29–38
8. G. Bolelli, V. Cannillo, L. Lusvarghi, M. Montorsi, F.P. Mantini, and M. Barletta, Microstructural and Tribological Comparison of HVOF-Sprayed and Post-Treated M-Mo-Cr-Si (M=Co, Ni) Alloy Coatings, *Wear*, 2007, **263**, p 1397–1416
9. J. Mateos, J.M. Cuetos, R. Vijande, and E. Fernandez, Tribological Properties of Plasma Sprayed and Laser Remelted 75/25 Cr_3C_2 /NiCr coatings, *Tribol. Int.*, 2001, **34**, p 345–351
10. G-Ch Ji, Ch-J Li, Y-Y. Wang, and W-Y. Li, Microstructural Characterization and Abrasive Wear Performance of HVOF sprayed Cr_3C_2 -NiCr Coating, *Surf. Coat. Technol.*, 2006, **200**, p 6749–6757
11. A. Strecker, U. Salzberger, and J. Mayer, Specimen Preparation for Transmission Electron Microscopy: Reliable Method for Cross-Sections and Brittle Materials, *Prakt. Metallogr.*, 1993, **30**, p 482–495
12. R. Viana and A.R. Machado, Influence of Adhesion Between Coating and Substrate on the Performance of Coated HSS Twist Drills, *J. Braz. Soc. Mech. Sci. Eng.*, 2009, **31**, p 327–332
13. P. Kutilek and J. Miksovsky, The Procedure of Evaluating the Practical Adhesion Strength of New Biocompatible Nano- and Micro-Thin Films in Accordance with International Standards, *Acta Bioeng. Biomech.*, 2011, **13**, p 87–94
14. E. Zdravecka, J. Suchanek, J. Tkacova, J. Trpcevska, K. Brinkiene, and K. Mechanika, Investigation of Wear Resistance of High Velocity Oxy-Fuel Sprayed WC-Co and Cr_3C_2 -NiCr Coatings, *Mechanika*, 2010, **84**, p 75–79
15. S. Hogmark, S. Jacobson, and M. Larsson, Design and Evaluation of Tribological Coatings, *Wear*, 2000, **246**, p 20–33
16. K. Kato, Wear in Relation to Friction- a Review, *Wear*, 2000, **241**, p 151–157